Atmos. Chem. Phys. Discuss., https://doi.org/10.5194/acp-2017-557
Manuscript under review for journal Atmos. Chem. Phys.
Discussion started: 21 June 2017

Atmospheric Chemistry and Physics Discussions

Assessing the ability to derive rates of polar middle-atmospheric descent using trace gas measurements from remote sensors

Niall J. Ryan[1], Douglas E. Kinnison[2], Rolando R. Garcia[2], Uwe Raffalski[3], Mathias Palm[1], Justus Notholt[1]

[1] Institute of Environmental Physics, University of Bremen, Bremen, 28359, Germany
[2] Atmospheric Chemistry Observations and Modeling Laboratory, National Center for Atmospheric Research, Boulder, Colorado, USA
[3] Swedish Institute of Space Physics, Box 812, SE-981 28 Kiruna, Sweden

Correspondence to: Niall J. Ryan (n_ryan@iup.physik.uni-bremen.de)

Abstract. We investigate the reliability of using trace gas measurements from remote sensing instruments to infer polar atmospheric descent rates during winter. Using output from the Specified Dynamics Whole Atmosphere Community Climate Model (SD-WACCM) between 2008 and 2014, tendencies of carbon monoxide (CO) concentrations are used to assess a common assumption of dominant vertical advection of tracers during polar winter. The results show that dynamical processes other than vertical advection are not negligible, meaning that the transport rates derived from trace gas measurements do not represent the mean descent of the atmosphere. The relative importance of vertical advection is lessened during periods directly before and after a sudden stratospheric warming. It was also found that CO chemistry cannot be ignored in the mesosphere due to the night-time layer of OH at approximately 80 km altitude. CO concentration data from the Kiruna Microwave Radiometer and the Microwave Limb Sounder are used in combination with the modelled CO tendencies to estimate errors involved in calculating the mean descent of the atmosphere from remote sensing measurements. The results indicate errors on the same scale as the calculated descent rates, and often a misinterpretation of the direction of air motion. We suggest an alternative definition of the rate calculated using remote sensing measurements: not as the mean descent of the atmosphere, but as an effective rate of vertical transport for the trace gas under observation.

1 Introduction

The rate of the descent of air above the poles during winter has been an area of interest for some time because it influences the transport of trace gases from the thermosphere to the middle atmosphere (mesosphere and stratosphere) (e.g., Plumb et al., 2002; Engel et al., 2006; Smith et al., 2011; Manney et al., 2009). This vertical branch of the meridional circulation can transport gases with high thermospheric concentrations, and change the composition of the middle-atmosphere (e.g., Solomon et al., 1982; Allen et al., 2000; Hauchecorne et al., 2007; Smith et al., 2011; Garcia et al., 2014; Manney et al., 2009, 2015). The downward transport of nitrogen oxide (NO), produced around 110 km through energetic particle precipitation (EPP) events (e.g. Barth and Bailey, 2004; Randall et al., 2005, 2007, 2015), garners particular attention

because NO_x ($NO + NO_2$) catalytically destroys ozone in the stratosphere. Periods of strong atmospheric descent are known to coincide with the timing of sudden stratospheric warmings (SSWs) (e.g. Manney et al., 2003, 2009; Siskind et al., 2010; Jackman et al., 2009, Holt et al., 2013). Elevated concentrations of carbon monoxide (CO) and NO_x have been observed to linger in the middle atmosphere when there is an exceptionally strong polar vortex after a strong SSW, helping to confine descending air at the pole (Randall et al., 2006). Randall et al. (2009) suggest that, in these cases, concentrations of EPP-produced NO_x are controlled more by mesosphere and lower thermosphere (MLT) descent rates than by the structure of the vortex. Siskind et al. (2016) found that due to downward transport of methane (CH_4) in years with strong, uninterrupted mesospheric descent, summertime upper stratospheric chlorine monoxide (ClO) is about 50 % greater than in years with strong horizontal transport.

A direct measurement of the mean vertical motion of air in the middle-atmosphere is currently not possible because of the small velocities, and so an analysis of changes in measured tracer (relatively long-lived trace gas) concentrations offers a means to indirectly observe the vertical motion. Another indirect determination can be made using the diabatic circulation approach (e.g., Dunkerton, 1978; Solomon et al., 1986; Medvedev and Fomichev, 1994) but this method is not discussed further here. The chemical lifetime of CO during polar night and the strong vertical gradient in its concentration make it a good tracer (Solomon et al., 1985; Allen et al., 1999; Lee et al., 2011). Water vapour (H_2O) is used to infer vertical motion (e.g., Straub et al., 2012) but a varying vertical gradient limits the altitudes at which it can be used (Lee et al., 2011). Nassar et al. (2005) used nitrous oxide (N_2O), CH_4, and H_2O to infer rates of vertical motion in the upper stratosphere and lower mesosphere, and Bailey et al. (2014) used a combination of NO, H_2O, and CH_4 to derive profiles of vertical motion in the middle atmosphere. A partial list of studies that have used tracers to calculate rates of vertical motion is given in Table 1, similar to Hoffman (2012) for studies using CO. The tracers used and the determined rates are also listed, along with the terminology used to describe the motion. The descent rates range from -100 m/day to -1200 m/day and show much variability, which can be expected as the studies are performed for different years and/or different times of the year, and at different locations (with the minus sign indicating descent rather than ascent).

A general assumption made in the derivations of the rates is that the observed change in a tracer concentration over time is caused by vertical advection. The assumption draws from the fact that the polar vortex edge acts as a barrier to lower latitude air and hinders horizontal mixing of air masses between the inside and outside of the vortex (Schoeberl et al., 1992, Manney et al., 1994), but limited mixing still occurs and defining the edges of the polar vortex is not straightforward. During the formation/breakdown of the polar vortex at the beginning/end of winter, the transport barrier is weaker and the location of the vortex edge becomes much less well-defined (Manney et al., 1997), making it more difficult to identify inner-vortex air masses. This is also true for SSW events where the vortex is weakened, or breaks down and reforms, allowing increased mixing (Manney et al., 2009, 2015). When the vortex is well established, the edge definitions that rely on wind fields (such as scaled potential vorticity (e.g., Manney et al., 1994, 2007, 2011; Jin et al.,2006)) become less reliable in the mesosphere where wind observations are uncommon and reanalysis winds are known to be fallible (Manney et al., 2008a, b; Rienecker et al., 2011).

The aim of this study is to assess the limits of the above assumption when using tracer measurements to derive rates of vertical motion in the middle atmosphere. The specified dynamics version of the Whole Atmosphere Community Climate Model (SD-WACCM) is used to determine the relative contributions to changes in CO concentrations during polar winter. The results are combined with measurements of CO from the Kiruna Microwave Radiometer (KIMRA) and the Microwave Limb Sounder (MLS) to estimate the error associated with descent rates calculated assuming pure vertical advection of the tracer. Three commonly used representations of the data are assessed: a local area above a specific location (Kiruna, in this case), a zonal mean at a certain latitude (80˚ N is used as an example), and a polar mean (60˚ - 90˚ N). The winters of 2008/2009 and 2010/2011 are used in the study as an example of a winter with a strong SSW and relatively quiet winter, respectively. This study could be performed using model output in place of the measured CO concentrations, but ground-based and satellite measurements are presented because the aim of the study is to evaluate a methodology that relies solely on data from instruments. The calculations were also performed using only model output (not shown), and the results lead to the same conclusion. This was expected due to the level of agreement between the modelled and measured CO (Sect. 2.4).

Section 2 outlines the instruments and the model used in this study as well as their datasets. A brief comparison of the three CO datasets is also provided. Section 3 investigates the trajectories of air parcels arriving in the Arctic during winter, and the evolution of the mean tendencies of CO concentrations in the Arctic middle atmosphere due to each component of the continuity equation. Section 4 shows the rates of vertical motion calculated using CO measurements and the above assumption, and estimates how these rates change when accounting for all parts of the continuity equation. Section 5 uses CO concentration tendencies from 2008 to 2014 to assess their relative importance during different months. Section 6 contains a discussion of the results and the limitations of the study, and suggests a different interpretation of the rates derived from tracer measurements. Section 7 provides concluding remarks.

2 Instruments, model, and data

2.1 KIMRA

KIMRA is a ground-based microwave remote sensor located at the Swedish Institute for Space Physics, Kiruna, Sweden (67.8˚ N, 20.4˚ E). The instrument is a passive remote sensor and radiances from atmospheric CO are measured at a frequency 230.54 GHz. Specific details on the instrument can be found in Raffalski et al. (2002) and Hoffman et al. (2011). The current CO dataset from KIMRA covers Arctic winters from 2008 to 2015 with gaps corresponding to instrument non-operation and summer periods when CO concentrations in the middle atmosphere are too low to be accurately measured. The average altitude range of the data is 46 – 86 km and the vertical resolution is 15 – 18.5 km, depending on the altitude. Details on the measurement technique and CO inversion scheme are given in Ryan et al. (2017). The average precision of wintertime KIMRA CO volume mixing ratios (VMRs) range from 0.06 ppm at 46 km altitude to 2.7 ppm at 86 km. KIMRA CO data presented in this work has been averaged to give daily profiles.

Atmos. Chem. Phys. Discuss., https://doi.org/10.5194/acp-2017-557
Manuscript under review for journal Atmos. Chem. Phys.
Discussion started: 21 June 2017

2.2 MLS

MLS is a microwave remote sensor aboard the Aura satellite, launched in July 2004, and is part of NASA's Earth Observing System. Atmospheric CO is retrieved from radiance measurement made in two bands of the 240 GHz radiometer. A description of the MLS instrument can be found in Waters et al. (2006) and details on the retrieval can be found in Pumphrey et al. (2007) and Livesey et al. (2008). The data used here is version 4.2 (Schwarz et al., 2015), which is described in Livesey et al. (2015). These CO profiles cover a pressure range of 215 – 0.0046 hPa and have a maximum (largest) precision of 11 ppm at the highest pressure level. For the data used here, the vertical resolution is between 3.8 and 6.2 km, and the horizontal resolution is between 200 and 250 km. MLS data presented here has been averaged to produce daily profiles.

2.3 SD-WACCM

The Community Earth System Model version 1 (CESM1), Whole Atmosphere Community Climate Model (WACCM), is a coupled chemistry climate model from the Earth's surface to the lower thermosphere (Marsh et al., 2013 and references therein). WACCM is a superset of the Community Atmosphere Model, version 4 (CAM4), and includes all of the physical parameterizations of CAM4 (Neale et al., 2013) and a finite volume dynamical core (Lin, 2004) for the tracer advection. The simulation of WACCM4 used in this study is run with specified dynamics (SD) fields, using meteorological analyses from the National Aeronautics and Space Administration (NASA) Global Modeling and Assimilation Office (GMAO) Modern-Era Retrospective Analysis for Research and Applications (MERRA) (Rienecker et al., 2011). The chemical component is based on version 3 of the Model for Ozone and Related Chemical Tracers (Kinnison et al, 2007). Garcia et al. (2014) discusses an update to the absorption cross section for O_2, which increased modelled CO mixing ratios in the MLT, bringing them closer to observations.

SD-WACCM constrains the atmosphere towards observations below 50 km through nudging with data from the above-mentioned analysed meteorological fields. Above 60 km the atmosphere is fully interactive and between 50 and 60 km the nudging linearly decreases to zero. Details on the nudging of the temperature and wind fields in the model can be found in Lamarque et al. (2012) and references therein. The model also tends towards observations at altitudes above 60 km because the zonal-mean mesospheric winds and temperatures at higher altitudes have been shown to be strongly constrained by the stratosphere (Liu et al., 2010; McLandress, 2013), but precise agreement cannot be expected.

For the model runs used in this work, the pressure grid consists of 88 layers from the ground to the thermosphere (~133 km). The altitude resolution of the grid increases from ~0.1 km near the surface to ~3.5 km in thermosphere. The horizontal resolution is 1.9° x 2.5° in latitude and longitude. Daily model output from 2008 to 2014 is used for this study.

2.4 CO VMR comparison

Because CO information from three sources is being used in this study, a brief comparison is called for. Figure 1 plots the CO VMRs from KIMRA, MLS, and SD-WACCM above Kiruna for 2008 through 2014. The aim of a comparison is to see

Atmos. Chem. Phys. Discuss., https://doi.org/10.5194/acp-2017-557
Manuscript under review for journal Atmos. Chem. Phys.
Discussion started: 21 June 2017

whether the datasets capture the same variability in middle-atmospheric CO. The VMRs are plotted at five altitudes between 46 and 86 km. This is the average altitude range of KIMRA CO data and reaches the upper altitude limit of MLS CO data. The MLS and SD-WACCM concentrations are also plotted after the profiles have been smoothed with the KIMRA averaging kernels (Rodgers and Connor, 2003). This method allows a meaningful comparison of datasets that have significantly different vertical resolutions. MLS data within ± 2° latitude and ± 10° longitude of Kiruna are used here. A more comprehensive comparison of KIMRA and MLS is given in Ryan et al. (2017). SD-WACCM data is here bilinearly interpolated to the location of Kiruna, but a significant change in the results isn't found when simply using the model coordinate grid point closest to Kiruna. The three CO datasets show agreement on seasonal and daily time scales. Agreement between the model and instruments on such time scales highlights the power of SD-WACCM as a tool for investigating trends as well as temporally short events in the atmosphere. Table 2 lists the correlation and regression coefficients calculated for each data pairing. Regression coefficients are calculated accounting for errors in the abscissa and ordinate variables (York et al., 2004), with a 15 % error assumed for SD-WACCM CO VMRs. Correlations between KIMRA and smoothed MLS, and KIMRA and smoothed SD-WACCM, are ≥ 0.86 at all altitudes, and MLS and SD-WACCM correlations are ≥ 0.88. MLS and SD-WACCM were compared at other polar locations (not shown here) and display similar agreement.

3 Contributions to the CO continuity equation

3.1 The TEM continuity equation

The mass transport of the residual mean meridional circulation is well represented by the Transformed Eulerian Mean (TEM) formulation (Andrews and McIntyre, 1976), and is covered in detail in Andrews et al. (1987). The TEM circulation in the solstice seasons is dominated by flow from the summer to the winter pole, accompanied by downward and upward transport above the winter and summer poles, respectively. The TEM zonal-mean tracer continuity equation has been described in various works (e.g., Garcia and Solomon, 1983; Andrews et al., 1987; Brasseur and Solomon, 2005; Monier and Weare, 2005; Smith et al., 2011):

$$\frac{\partial \bar{\chi}}{\partial t} = -\overline{w^*}\frac{\partial \bar{\chi}}{\partial z} - \overline{v^*}\frac{\partial \bar{\chi}}{\partial y} + \bar{S} + \overline{X_{mol}} + \frac{1}{\rho_0}\nabla \cdot M + \overline{\frac{1}{\rho_0}\frac{\partial}{\partial z}\left(\rho_0 K_{zz}\frac{\partial \chi}{\partial z}\right)}, \quad (1)$$

where χ is the CO VMR, $\overline{w^*}$ is the vertical component of the residual mean meridional circulation, and $\overline{v^*}$, is the horizontal component. $\bar{S}$ is the zonal-mean net chemical production of CO and $\overline{X_{mol}}$ is the zonal-mean molecular diffusion of CO. $\nabla \cdot M$ is the divergence of the resolved eddy flux vector and describes the eddy transport of CO, with ρ_0 as the basic density. K_{zz} is the diffusion coefficient due to unresolved small-scale gravity wave breaking, and the last component of Eq. (1) represents the transport of CO due to parameterised eddy flux divergence (from gravity waves). The right-hand-side (RHS) terms of Eq. (1) are calculated using daily output from SD-WACCM and details on the exact equations can be found in Andrews et

al. (1987). The value of K_{zz} calculated with SD-WACCM depends, among other things, upon the assumed Prandtl number, which describes the ratio of the eddy momentum flux to the eddy flux of chemical species (Garcia et al., 2007). The Prandtl number is 2 for the model runs in this work (see Section 6). Finite differences in Eq. (1) are calculated as centred differences except at the boundaries of grids, where forward and backward differences are used.

The terms of Eq. (1) are rewritten here as:

$$\frac{\partial \overline{\chi}}{\partial t} = adv\_w * + adv\_v * + chem + Xmol + Xedd + Xk_{zz}, \quad (2)$$

to simply express the tendencies of CO in the continuity equation. The change in zonal-mean CO VMR with time is a sum of the contributions from (following the RHS of Eq. (2)): vertical advection, horizontal advection, net chemical production, molecular diffusion, eddy transport, and unresolved eddy transport, which, for present purposes, is due to gravity waves.

3.2 Trajectories during Arctic winter

As a first step to examine the assumption of purely vertical tracer advection, the back-trajectories of air parcels during two Arctic winters are plotted in Figure 2. The parcels arrive at 5 altitudes between 46 and 86 km and at two locations, 67˚ N and 80˚ N. They are advected, from these locations, backwards in time over 60 days, in 4 hour steps, using $\overline{w}*$ and $\overline{v}*$. The starting date for the trajectory calculations (arrival date of the air parcels) is February 28th, for 2009 and 2011. The winter of 2009 had a major SSW (during which the 10 hPa zonal circulation becomes easterly at 60˚ N) beginning on the 24th January, and 2011 had a relatively stable vortex throughout the winter. The results in Figure 2 are consistent with similar calculations in Smith et al. (2011) and Straub et al. (2012), for the general shape of the trajectory and in that the parcels do not originate above approximately 100 km. The parcels at 80˚ N arrive from higher altitudes due to a stronger vertical component of the circulation compared to 67˚ N. Conversely, the horizontal component of the circulation is stronger at 67˚ N and the parcels arriving there originate from lower latitudes compared to those arriving at 80˚ N. A clear reversal of the trajectory around the time of the SSW can be seen for the air parcel arriving at 66 km altitude, 80˚ N, because of temporary changes in the direction of $\overline{w}*$ and $\overline{v}*$. These changes cause the air parcel to reverse direction before starting to descend again. It is evident from Figure 2 that the circulations at the pole have varying degrees of vertical and horizontal components.

3.3 Tendencies of CO during Arctic winter

Figure 3 plots the wintertime tendencies of CO (RHS of Eq. (2)) for 2008/2009 and 2010/2011. The zonal mean tendencies are shown for 67˚ N, 80˚ N, and a north pole average (60˚ – 90˚ N), and are plotted as an 11-day running mean. In the context of a point measurement at Kiruna, a full rotation of the vortex is on the order of 10 days (assuming a zonal wind speed of 20 m/s at 67˚ N). Relevant comments on the results are provided here but an in-depth analysis is not made as it is not the focus of the study. Molecular diffusion ($Xmol$) generally causes negligible changes in CO, compared to other process, below approximately 85 km. Unresolved eddy transport (Xk_{zz}) is also negligible below approximately 75 km. Both processes tend to cause a decrease in CO VMRs throughout the winter, agreeing with results of Smith et al. (2011). Changes

in CO due to chemistry ($chem$) are small below approximately 70 km, but all cases show a sustained sink for CO during the winter in a layer at around 80 km altitude. The layer coincides with the location of a night-time layer of hydroxyl (OH) around 82 km altitude (Brinksma et al., 1998, Pickett et al., 2006, Damiani et al., 2010). OH is known as the dominant chemical sink for middle-atmospheric CO (Solomon et al, 1985). $chem$ tendencies are stronger at 80° N than 67° N, with magnitudes reaching more than 0.3 ppm/day. The results suggest that CO chemistry cannot be ignored in the mesosphere during winter. Tendencies due to resolved eddy diffusion ($Xedd$) are the most variable, and more so at 67° N than 80° N because of proximity to the edge of the polar vortex. The polar average shows that $Xedd$ generally reduces CO concentrations during the winter. The largest tendency in CO is from vertical advection (adv_w*), and causes an almost constant increase in CO VMRs throughout the winter, before reversing when the TEM vertical wind changes direction in Spring (visible in all adv_w* plots). The tendency is stronger at 80° N compared to 67° N due to a stronger vertical component of the residual circulation at the higher latitude (Smith et al., (2011), and see Figure 2). A signature of the major SSW in 2009 can be seen in the adv_w* tendency for that year, with a decrease and eventual change to a negative tendency. For some time directly afterwards, the tendency has a stronger positive magnitude than before. This agrees with observations of stronger vertical motion above the pole after a SSW (see references in Table 1). There is also a brief change to a positive adv_w* at 80 N, around 80 km altitude, in early January 2011. This coincides with a relatively strong positive value for $Xedd$ at the same time and location, indicating strong wave activity. The tendency from horizontal advection (adv_v*) is negative almost everywhere. This is expected, considering the direction of $\overline{v*}$ during winter and the low-to-high gradient of CO from lower to higher latitudes. The magnitude of the tendency decreases in spring but a change of sign is not obvious by the end of April. At 67° N, the magnitudes of adv_v* are roughly half that of adv_w*, and at 80° N they are roughly one fifth. Considering this observation alone, changes in CO VMRs cannot be attributed solely to vertical advection.

4 Rates of vertical motion with KIMRA and MLS

In this section, the rates of vertical motion are calculated using CO data from KIMRA and MLS, by two methods. The first method assumes that observed changes in CO VMRs are due to vertical advection alone. This is a commonly used method (see Table 1) and involves tracking the altitude of a chosen concentration of CO over time and then performing a linear regression on the data of altitude (z) vs. time (t). The rate for a given date is calculated here by performing a regression on the CO data within ±5 days of the date. This gives an 11-day running mean of the rate of vertical motion. The calculation can be done for multiple concentrations, to retrieve a vertical profile of the rates of vertical motion, as in Bailey et al. (2014). The term used here to denote the rate of vertical motion calculated using CO concentration is w_{CO}, following Hoffman (2012). The second method used here includes information on changes in CO VMRs due to all terms of the continuity equation in Sect. 2. Before tracking a CO concentration from one time step to the next, the concentration is adjusted using the tendencies of the continuity equation, except for adv_w*, for the corresponding time frame. This accounts for changes in CO concentration from other processes as one tracks its movement due to vertical advection. The resulting rate is called

Atmos. Chem. Phys. Discuss., https://doi.org/10.5194/acp-2017-557
Manuscript under review for journal Atmos. Chem. Phys.
Discussion started: 21 June 2017

Atmospheric Chemistry and Physics Discussions

w_{CO} *corrected*. This could be considered a crude approach, combining instrument data and model output, but the aim here is to provide an estimate of the errors that can be incurred by neglecting influences on CO other than vertical advection. To illustrate the difference between w_{CO} and w_{CO} *corrected*, example algebraic expressions for the rates between a time step *n* and *n+1* are given Eq. (3), (4), and (5). In practice, w_{CO} and w_{CO} *corrected* were calculated by performing a linear regression on the 11-day altitude vs. time data, including errors in the estimated altitude of the measured CO concentrations.

$$w_{CO}(z,t) = \frac{z_{n+1}-z_n}{t_{n+1}-t_n}\Big|_{\bar{\chi}} \quad (3)$$

$$w_{CO}\ corrected(z,t) = \frac{z(\bar{\chi}_{n+1})-z(\bar{\chi}_n)}{t_{n+1}-t_n} \quad (4)$$

where,

$$\bar{\chi}_{n+1} = \bar{\chi}_n + \left(\frac{1}{2}\sum_{i=n}^{n+1}[adv\_v * + chem + Xmol + Xedd + Xk_{zz}]\right)(t_{n+1} - t_n) \quad (5)$$

The results for winters 2008/2009 and 2010/2011 are plotted in Fig 4. For each winter, w_{CO} and w_{CO} *corrected* are calculated as: a local value above Kiruna using KIMRA data, a zonal mean at 80˚ N using MLS data, and a polar mean (60˚ – 90˚ N) using MLS data. The methods above were found to be unreliable when there are very low CO VMRs, and gave unrealistic rates of motion. This was more likely to occur at lower altitudes where CO VMRs are relatively low. Sometimes a CO concentration could not be followed within the specified altitude range (no extrapolation was used) and so there are a few locations with no rate information. The differences between the two rates, w_{CO} *corrected* $- w_{CO}$, are also shown in Fig. 4.

The values of w_{CO} are generally of a smaller magnitude than w_{CO} *corrected* during winter, meaning that the derived rates of descent are stronger when accounting for CO tendencies other than vertical advection. This makes sense because, as seen in Figure 3, the other transport terms of the continuity equation (and the chemical loss term) tend to oppose the vertical advection term. The differences between the two rates are often of the same order as w_{CO}. The sign of w_{CO} and w_{CO} *corrected* are often opposite, meaning the calculated direction of air motion is prone to change when accounting for CO tendencies other than vertical advection. In each example for 2008/2009, the magnitude of the positive (upward) motion around the time of SSW is decreased for w_{CO} *corrected* compared to w_{CO}. After the SSW, and into March, the strongest descent values are seen around 70 – 80 km in w_{CO} *corrected*, compared to values of ascent seen in w_{CO} at the same location. The results indicate that the "true" rate of atmospheric descent is masked by sinks of CO, and by transport processes that oppose the tendency due to vertical advection.

5 Relative strengths of CO tendencies, by month

To give an idea of the relative influence each tendency has on middle-atmospheric CO concentrations each month, daily CO tendencies from 2008 to 2014 are used to provide relative values of their monthly mean. For a given tendency, the daily values are separated by calendar month and averaged, to give a monthly mean tendency. The same is done for the absolute

sum of all tendencies, to give a monthly mean absolute sum. The monthly mean tendencies are then normalised by the monthly mean absolute sum, and will be referred to here as relative strengths. Using an absolute sum for normalisation retains the sign of the individual tendencies and avoids a large spread in the results when there is a small denominator (i.e., when the tendencies cancel each other and their sum is near zero). The relative strength of the sum of all tendencies, excluding adv_w*, is also included as a variable. This variable will be referred to here as "*other processes*" and can be directly compared to the relative strength of adv_w*, to judge the influence of vertical advection compared to all other processes. The results are shown for the north pole (60˚ – 90˚ N) in Fig. 5, and the south pole (60˚ – 90˚ S) in Fig. 6. For the north pole, tendencies corresponding to 10 days directly before and after a SSW (starting on January 22nd, 24th, and 26th, 2008, 2009, 2011, respectively, and February 6th, 2013) are excluded from the calculation, as well as the start-date. Ten days was chosen to remove effects directly before and after a SSW, but signatures of the events remain in the data. The information from before and after an SSW is used to separately calculate the relative strengths for these times and is shown in Fig. 7.

For the north pole average in Fig. 5, The relative strength of *other processes* is everywhere negative from October to March and the relative strength of adv_w* is positive. Both adv_w* and *other processes* show a change of sign in April. The relative strength of adv_w* reaches a maximum value of 0.8 at lower altitudes in October and November, and decreases with altitude to approximately 0.5 at 86 km for these months. The relative strength of *other processes* shows an opposite trend: negative values strengthening with altitude to approximately -0.4. At the lower limit of the altitude range in January, adv_w* shows a lower relative strength than *other processes* due to a strong $Xedd$ influence. This is likely the "left-over" influence of the SSWs in the data. By March, the relative strength of *chem* is prominent below 65 km, and the magnitude of adv_w* is matched by *other processes*. By April, the residual mean circulation has reversed direction and adv_w* has changed sign at most altitudes. The negative value of *chem* is then dominant at lower altitudes, and there is a stronger positive tendency above ~80 km (from photolysis of carbon dioxide (CO_2)). There are no months where the relative strength of *other processes* can be considered negligible compared to the relative strength of adv_w*. The results for the south pole, in Fig. 6, are qualitatively similar to the north pole. The relative strength of adv_w* shows a maximum of ~0.8. Both hemispheres show a peak in *chem* at 80 km for most of winter. The relative strength of $Xedd$ is not as prominent at the south pole as the north, likely due to the higher stability of the southern polar vortex. For the 10 days directly before and after SSWs, in Fig. 7, the relative strength of adv_w* is less than 0.5 at all altitudes. $Xedd$ is strong below 60 km, such that the relative strength of *other processes* has a larger magnitude than that of adv_w* at many altitudes. The relative strength of adv_w* shows a more oscillatory structure with altitude, and there is a local minimum at about 70 km in the data for 10 days after SSWs. There is also a positive peak in the relative strength of Xk_{zz} after SSWs at this altitude.

Atmos. Chem. Phys. Discuss., https://doi.org/10.5194/acp-2017-557
Manuscript under review for journal Atmos. Chem. Phys.
Discussion started: 21 June 2017

6 Discussion

The results of the previous sections are clear on one point, that the assumption of observed changes in CO concentrations being solely due to vertical advection is not a valid one. What is not obvious, is what the rates inferred from the behaviour of tracer isolines (w_χ, under the nomenclature used here) represent. When making observations on timescales of weeks, the TEM offers a suitable representation of the governing dynamics. The vertical velocities calculated by observing CO, however, fall short of the magnitudes of the TEM vertical wind, $\overline{w*}$, found with SD-WACCM. Figure 8 shows the polar average (60° – 90° N) $\overline{w*}$ for winters of 08/09 and 10/11, calculated using daily SD-WACCM data. Comparing this to the values of w_{CO} and w_{CO} *corrected* in Figure 4, it is clear that the rates derived from CO values are generally of lower magnitude than $\overline{w*}$. This agrees with the results of Hoffman (2012). w_{CO} *corrected* more closely matches the sign and general pattern of $\overline{w*}$, but does not reach the semi-persistent descent rates of 1.2 km/day between 60 and 70 km, or the magnitude of the enhanced rate of descent (> 1.6 km/day) after the SSW in 2009. Similar results are observed when using SD-WACCM CO profiles to derive vertical velocity, instead of KIMRA and MLS data (not shown here).

Some of the difference may be attributed to the time resolution, or assumed parameters, of the SD-WACCM output used in this work. Meraner and Schmidt (2016) showed that the tendency of NO due to $\overline{w*}$ can be quite different (> 1 ppm/day at 90 km) when calculated using 6-hourly output or daily output from HAMMONIA (Hamburg Model of the Neutral and Ionized Atmosphere)). Meraner et al. (2016) showed that NO_x transport in the mesosphere is highly sensitive to the strength of the gravity wave source. The amplitude of gravity waves influence the altitude at which the waves break and deposit their momentum, which in turn affects the vertical profile of $\overline{w*}$. Garcia et al. (2014) found that using a Prandtl number of 4 for WACCM, instead of 2 (as used here), gave better agreement with polar CO profiles from satellite instruments (the Atmospheric Chemistry Experiment Fourier Transform Spectrometer (ACE-FTS) on SCISAT-1, and the Michelson Interferometer for Passive Atmospheric Sounding (MIPAS) on Envisat). The opposite was found for tropical and mid-latitude CO profiles, and Garcia et al. (2014) consider that deficiencies in the modelling of diffusive eddy transport may be due to problems in producing the correct latitudinal profile of K_{zz}, which cannot be addressed by simply adjusting the Prandtl number.

As the results here indicate that the commonly used approximation of $\overline{w*}$ with w_χ (from measurement data only) is not valid, we suggest an alternative interpretation of w_χ: as an effective rate of vertical transport for the trace gas χ. The interpretation still concerns the descent of a tracer through the middle atmosphere, but allows for a chemical sink, or for processes other than vertical advection to influence the descent rate, e.g., horizontal advection or an increase in unresolved eddy transport after a SSW. Hoffman (2012) put forward a similar interpretation for w_{CO}, but with an assumption that the overall dynamic effects on CO are representative for the complete mesospheric air, and so w_{CO} is representative of w_χ for all tracers. The results here do not confirm that assumption, as it would require tracers to have the same horizontal and vertical concentration gradients (see Sect. 2.5 and references therein). The consistent negative chemical tendency of CO, seen here in

a layer around approximately 80 km, also indicates the need to account for the behaviour of chemical sinks, even during polar night.

7. Conclusion

The aim of this work was to assess how well polar atmospheric descent rates can be derived from remote sensing measurements of atmospheric trace gases. Tendencies of middle atmospheric CO were calculated using output from SD-WACCM for the years 2008 to 2014, and used to evaluate the relative influence of processes involved in the TEM CO continuity equation. The results show that dynamical processes other than vertical advection cause non-negligible changes in CO concentrations during winter, and particularly directly before and after sudden stratospheric warmings. The results also show a chemical sink for CO, present throughout polar night, due to the layer of night-time OH at approximately 80 km. CO data from the ground-based radiometer, KIMRA, and satellite-borne radiometer, MLS, were used in combination with the tendency data to estimate the errors involved in assuming pure vertical advection of CO. Rates of atmospheric motion were calculated when assuming only vertical advection, and corrected rates were calculated by including model information for all processes. The differences between the two results are of the same order as the calculated rates, and the rates often show opposite directions for the mean vertical wind. The corrected rates more closely match the TEM vertical wind velocity from SD-WACCM, but both results using CO show smaller magnitudes relative to the TEM vertical wind, in agreement with previous work. Monthly mean relative tendencies for CO show that there are no months during polar winter when vertical mean advection dominates the budget of CO to such an extent that vertical mean velocity can be accurately derived.

A commonly used approximation of the vertical mean velocity of the atmosphere, $\overline{w*}$, using tracer (CO in this case) isolines is found to be invalid, and an alternative interpretation of the rates derived from trace gas measurements is suggested: an effective rate of vertical transport for the given trace gas. Such an interpretation still concerns the descent of trace gases from the mesosphere and thermosphere, but allows for chemical sinks, and changes in concentration from dynamical processes other than vertical advection. Due to possible differences in the behaviour of chemical sinks and concentration gradients, it is not clear whether the rate of vertical transport for one tracer is representative of the rate for another.

Author contributions

Mathias Palm and Niall J. Ryan designed the project. Douglas E. Kinnison performed the SD-WACCM runs and provided the output. Rolando R. Garcia provided scripts to calculate TEM variables from WACCM output. Uwe Raffalski maintains and operates KIMRA, and provided the instrument spectra. Niall J. Ryan performed the study with valuable insight and interpretation of results provided Douglas E. Kinnison and Rolando R. Garcia. Justus Notholt oversaw project development. Niall J. Ryan prepared the paper with contributions from coauthors.

Competing interests

The authors declare that they have no conflict of interest.

Acknowledgements

A 3-month research stay by Niall J. Ryan at the National Centre for Atmospheric Research, Boulder, Colorado, was funded by the University of Bremen, under the German Excellence Initiative (ABPZuK-03/2014). Instrument data used in the project was developed and acquired through funding from the German Federal Ministry of Education and Research (BMBF) through the research project: Role Of the Middle atmosphere in Climate (ROMIC), sub-project ROMICCO, project number 01LG1214A. The publication was supported through ROMICCO. We would like to thank the National Centre for Atmospheric Research (NCAR) for being so accommodating. The National Center for Atmospheric Research is sponsored by the US National Science Foundation. We express our gratitude to the MLS team for making their data available.

References

Allen, D. R., Stanford, J. L., López-Valverde, M. A., Nakamura, N., Lary, D. J., Douglass, A. R., Cerniglia, M. C., Remedios, J. J., and Taylor F. W.: Observations of Middle Atmosphere CO from the UARS ISAMS during the Early Northern Winter 1991/92, J. Atmos. Sci., 56(4), 563–583, 1999.

Andrews, D. G., and McIntyre, M. E.: Planetary waves in horizontal and vertical shear: The generalized Eliassen-Palm relation and mean zonal acceleration, J. Atmos. Sci., 33, 2031–2048, 1976.

Andrews, D., Holton, J., and Leovy, C.: Middle Atmosphere Dynamics, Academic Press, 489 pp., 1987.

Bailey, S. M., Thurairajah, B., Randall, C. E., Holt, L., Siskind, D. E., Harvey, V. L., Venkataramani, K., Hervig, M. E., Rong, P., and Russell III, J. M.: A multi tracer analysis of thermo- sphere to stratosphere descent triggered by the 2013 Stratospheric Sudden Warming, Geophys. Res. Lett., 41, 5216–5222, doi:10.1002/2014GL059860, 2014.

Barth, C. A., and Bailey S. M.: Comparison of a thermospheric photochemicalmodel with SNOE observations of nitric oxide, J. Geophys. Res., 109, A03304, doi:10.1029/2003JA010227, 2004.

Brasseur, G. and Solomon, S.: Aeronomy of the Middle Atmosphere: Chemistry and Physics of the Stratosphere and Mesosphere, Springer, 644 pp., 2005.

Brinksma, E. J., Meijer, Y. J., McDermid, I. S., Cageao, R. P., Bergwerff, J. B., Swart, D. P. J., Ubachs, W., Matthews, W. A., Hogervorst, W., and Hovenier, J. W.: First lidar observations of mesospheric hydroxyl, Geophys. Res. Lett., 25, 51-54, 1998.

Damiani, A., Storini, M., Santee, M. L., and Wang, S.: Variability of the nighttime OH layer and mesospheric ozone at high latitudes during northern winter: influence of meteorology, Atmos. Chem. Phys., 10, 10291-10303, doi:10.5194/acp-10-10291-2010, 2010.

Di Biagio, C. D., Muscari, G., di Sarra, A., de Zafra, R. L., Eriksen, P., Fiocco, G., Fiorucci, I., and Fu`a, D.: Evolution of temperature, O_3, CO, and N_2O profiles during the exceptional 2009 Arctic major stratospheric warming observed by lidar and mm-wave spectroscopy at Thule (76.5° N, 68.8° W), Greenland, J. Geophys. Res., 115, D24315, doi:10.1029/2010JD014070, 2010.

Dunkerton, T: On the mean meridional mass motions of the stratosphere and mesosphere, J. Atmos. Sci., 25, 2325-2333, 1978.

Engel, A., Möbius, T., Haase, H.-P., Bönisch, H., Wetter, T., Schmidt, U., Levin, I., Reddmann, T., Oelhaf, H., Wetzel, G., Grunow, K., Huret, N., and Pirre, M.: Observation of mesospheric air inside the arctic stratospheric polar vortex in early 2003, Atmos. Chem. Phys., 6, 267-282, doi:10.5194/acp-6-267-2006, 2006.

Forkman, P., Eriksson, P., and Murtagh, D.: Observing the vertical branch of the mesospheric circulation at lat N60° using ground based measurements of CO and H_2O, J. Geophys. Res., 110, 107, doi:10.1029/2004JD004916, 2005.

Funke, B., López-Puertas, M., García-Comas, M., Stiller, G. P., von Clarmann, T., Höpfner, M., Glatthor, N., Grabowski, U., Kellmann, S., and Linden, A.: Carbon monoxide distributions from the upper troposphere to the mesosphere inferred from

4.7 μm non-local thermal equilibrium emissions measured by MIPAS on Envisat, Atmos. Chem. Phys., 9, 2387–2411, doi:10.5194/acp-92387-2009, 2009.

Garcia, R. R. and Solomon, S.: A Numerical Model of the Zonally Averaged Dynamical and Chemical Structure of the Middle Atmosphere, J. Geophys. Res., 88, 1379–1400, doi:10.1029/JC088iC02p01379, 1983.

Garcia, R., Marsh, D., Kinnison, D., Boville, B., and Sassi, F.: Simulation of secular trends in the middle atmosphere, 1950-2003, J. Geophys. Res., 112, D09301, doi:10.1029/2006JD007485, 2007.

Garcia, R. R., López-Puertas M., Funke D., Marsh D. R., Kinnison D. E., Smith A. K., and González-Galindo F.: On the distribution of CO2 and CO in the mesosphere and lower thermosphere, J. Geophys. Res., 119, 5700–5718, doi:10.1002/2013JD021208, 2014.

Hauchecorne, A., Bertaux, J. -L., Dalaudier, F., Russell III, J. M., Mlynczak, M. G., Kyrölä, E., and Fussen, D.: Large increase of NO_2 in the north polar mesosphere in January–February 2004: Evidence of a dynamical origin from GOMOS/ENVISAT and SABER/TIMED data, Geophys. Res. Lett., 34, L03810, doi:10.1029/2006GL027628, 2007.

Hoffmann, C. G., Raffalski, U., Palm, M., Funke, B., Golchert,
S. H. W., Hochschild, G., and Notholt, J.: Observation of stratomesospheric
CO above Kiruna with ground-based microwave radiometry – retrieval and satellite comparison, Atmos. Meas. Tech., 4, 2389–2408, doi:10.5194/amt-4-2389-2011, 2011.

Holt, L. A., Randall, C. E., Peck, E. D., Marsh, D. R., Smith, A. K., and Harvey, V. L.: The influence of major sudden stratospheric warming and elevated stratopause events on the effects of energetic particle precipitation in WACCM, J. Geophys. Res., 118, 636–646, 2013.

Jackman, C. H., Marsh, D. R., Vitt, F. M., Garcia, R. R., Randall, C. E., Fleming, E. L., and Frith S. M.: Long-term middle atmospheric influence of very large solar proton events, J. Geophys. Res., 114, D11304, doi:10.1029/2008JD011415, 2009.

Jin, J. J., Semeniuk, K., Manney, G. L., Jonsson, A. I., Beagley, S. R., McConnell, J. C., Dufour, G., Nassar, R., Boone, C. D., Walker, K. A., Bernath, P. F., and Rinsland, C. P.: Severe Arctic ozone loss in the winter 2004/2005: observations from ACE-FTS, Geophys. Res. Lett., 33, L15801, 2006.

Kinnison, D. E., Brasseur, G. P., Walters, S., Garcia, R. R., Marsh, D. R., Sassi, F., Harvey, V. L., Randall, C. E., Emmons, L., Lamarque, J. F., Hess, P., Orlando, J. J., Tie, X. X., Randel, W., Pan, L. L., Gettelman, A., Granier, C., Diehl, T., Niemeier, U., and Simmons, A. J.: Sensitivity of chemical tracers to meteorological parameters in the MOZART-3 chemical transport model, J. Geophys. Res., 112, D20302, doi:10.1029/2006JD007879, 2007.

Lamarque, J.-F., Emmons, L. K., Hess, P. G., Kinnison, D. E., Tilmes, S., Vitt, F., Heald, C. L., Holland, E. A., Lauritzen, P. H., Neu, J., Orlando, J. J., Rasch, P. J., and Tyndall, G. K.: CAM-chem: description and evaluation of interactive atmospheric chemistry in the Community Earth System Model, Geosci. Model Dev., 5, 369–411, doi:10.5194/gmd-5-369-2012, 2012.

Lee, J. N., Wu, D. L., Manney, G. L., Schwartz, M. J., Lambert, A., Livesey, N. J., Minschwaner, K. R., Pumphrey, H. C., and Read, W. G.: Aura Microwave Limb Sounder observations of the polar middle atmosphere: Dynamics and transport of CO and H2O, J. Geophys. Res., 116, D05110, doi:10.1029/2010JD014608, 2011.

Lin, S. –J.: A "vertically-Lagrangian" finite-volume dynamical core for global atmospheric models. Mon. Wea. Rev., 132, 2293-2307, 2004.

Livesey, N. J., Filipiak, M. J., Froidevaux, L., et al.: Validation of Aura Microwave Limb Sounder O_3 and CO observations in the upper troposphere and lower stratosphere, J. Geophys. Res., 113, D15S02, doi:10.1029/2007JD008805, 2008.

Livesey, N. J., Read, W. G., Wagner, P. A., Froidevaux, L., Lambert, A., Manney, G. L., Millán Valle, L. F., Pumphrey, H. C., Santee, M. L., Schwartz, M. J., Wang, S., Fuller, R. A., Jarnot, R. F., Knosp, B. W., and Martinez, E.: Version 4.2x Level 2 data quality and description document, Tech. rep., Jet Propulsion Laboratory, 2015.

Liu, H., Foster, B. T., Hagan, M. E., McInerney, J. M., Maute, A., Qian, L., Richmond, A. D., Roble, R. G., Solomon, S. C., Garcia, R. R., Kinnison, D., Marsh, D. R., Smith, A. K., Richter, J., Sassi, F., and Oberheide, J.: Thermosphere extension of the Whole Atmosphere Community Climate Model, J. Geophys. Res., 115, A12302, doi:10.1029/2010JA015586, 2010.

Manney, G. L., Zurek, R. W., O'Neill, A., Swinbank, R., Kumer, J. B., Mergenthaer, J. L., and Roche A. E.: Stratospheric warmings during February and March 1993, Geophys. Res. Lett., 21, 813-816, 1994.

Manney, G. L., Daffer, W. H., Zawodny, J. M., Bernath, P. F., Hoppel, K. W., Walker, K. A., Knosp, B. W., Boone, C., Remsberg, E. E., Santee, M. L., Harvey, V. L., Pawson, S., Jackson, D. R., Deaver, L., McElroy, C. T., McLinden, C. A., Drummond, J. R., Pumphrey, H. C., Lambert, A., Schwartz, M. J., Froidevaux, L., McLeod, S., Takacs, L. L., Suarez, M. J., Trepte, C. R., Cuddy, D. C., Livesey, N. J., Harwood, R. S., and Waters, J. W.: Solar occultation satellite data and derived meteorological products: sampling issues and comparisons with Aura Microwave Limb Sounder, J. Geophys. Res., 112, D24S50, doi:10.1029/2007JD008709, 2007.

Manney, G. L., Krüger, K., Pawson, S., Minschwaner, K., Schwartz, M. J., Daffer, W. H., Livesey, N. J., Mlynczak, M. G., Remsberg, E. E., Russell, J. M., and Waters, J. W.: The evolution of the stratopause during the 2006 major warming: Satellite data and assimilated meteorological analyses, J. Geophys. Res., 113, D11115, doi:10.1029/2007JD009097, 2008b.

Manney, G. L., Daffer, W. H., Strawbridge, K. B., Walker, K. A., Boone, C. D., Bernath, P. F., Kerzenmacher, T., Schwartz, M. J., Strong, K., Sica, R. J., Krüger, K., Pumphrey, H. C., Lambert, A., Santee, M. L., Livesey, N. J., Remsberg, E. E., Mlynczak, M. G., and Russell III, J. R.: The high Arctic in extreme winters: vortex, temperature, and MLS and ACE-FTS trace gas evolution, Atmos. Chem. Phys., 8, 505-522, doi:10.5194/acp-8-505-2008, 2008a.

Manney, G. L., Schwartz, M. J., Krüger, K., Santee, M. L., Pawson, S., Lee, J. N., Daffer, W. H., Fuller, R. A., and Livesey, N. J.: Aura Microwave Limb Sounder observations of dynamics and transport during the record-breaking 2009 Arctic stratospheric major warming, Geophys. Res. Lett., 36, L12815, doi:10.1029/2009GL038586, 2009.

Manney, G. L., Lawrence, Z. D., Santee, M. L., Read, W. G., Livesey, N. J., Lambert, A., Froidevaux, L., Pumphrey, H. C., and Schwartz, M. J.: A minor sudden stratospheric warming with a major impact: Transport and polar processing in the 2014/2015 Arctic winter, Geophys. Res. Lett., 42, 7808–7816, doi:10.1002/2015GL065864, 2015.

McLandress, C., Scinocca, J. F., Shepherd, T. G., Reader, M. C., and Manney, G. L.: Dynamical control of the mesosphere by orographic and non-orographic gravity wave drag during the extended northern winters of 2006 and 2009, J. Atmos. Sci., 70, 2152–2161, 2013.

Medvedev, A. S. and Fomichev, V. I.: Net radiative heating and diagnostics of the diabatic circulation in the 15–110 km height layer, 56, 12, 1574-1581, doi: https://doi.org/10.1016/0021-9169(94)90087-6, 1994.

Meraner, K. and Schmidt, H.: Transport of nitrogen oxides through the winter mesopause in HAMMONIA.: J. Geophys. Res. Atmos., 121, 6, 2556–2570, doi:10.1002/2015JD024136, 2016.

Meraner, K., Schmidt, H., Manzini, E., Funke, B., and Gardini A.: Sensitivity of simulated mesospheric transport of nitrogen oxides to parameterized gravity waves, J. Geophys. Res. Atmos., 121, 12045–12061, doi:10.1002/2016JD025012, 2016.

Monier, E. and Weare, B. C.: Climatology and trends in the forcing of the stratospheric ozone transport, Atmos. Chem. Phys., 11, 6311-6323, doi:10.5194/acp-11-6311-2011, 2011.

Nassar, R., Bernath, P. F., Boone, C. D., Manney, G. L., McLeod, S. D., Rinsland, C. P., Skelton, R., and Walker, K. A.: ACE-FTS measurements across the edge of the winter 2004 Arctic vortex, Geophys. Res. Lett., 32, L15S05, doi:10.1029/2005GL022671, 2005.

Neale, R., Richter, J., Park, S., Lauritzen, P., Vavrus, S., Rasch, P., and Zhang, M.: The mean climate of the Community Atmosphere Model (CAM4) in forced SST and fully coupled experiments. J. Climate, 26, 5150–5168, 2013.

Pickett, H. M., Read, W. G., Lee, K. K., and Yung, Y. L.: Observation of night OH in the mesosphere, Geophys. Res. Lett., 33, L19808, doi:10.1029/2006GL026910, 2006.

Plumb, R. A., Heres W., Neu, J. L., Mahowald, N. M., del Corral, J., Toon, G. C., Ray, E., Moore, F., and Andrews, A. E.: Global tracer modeling during SOLVE: High-latitude descent and mixing, J. Geophys. Res., 107, 8309, doi:10.1029/2001JD001023, 2002.

Pumphrey, H. C., Filipiak, M. J., Livesey, N. J., Schwartz, M. J., Boone, C., Walker, K. A., Bernath, P., Ricaud, P., Barret, B., Clerbaux, C., Jarnot, R. F., Manney, G. L., and Waters, J. W.: Validation of middle-atmosphere carbon monoxide retrievals from MLS on Aura, J. Geophys. Res., 112, D24S38, doi:10.1029/2007JD008723, 2007.

Raffalski, U., Berg, H., Hochschild, G., and Kopp, G.: Continuous ozone measurements over Kiruna during winter/spring 2002: A new millimeter wave radiometer operated at the Swedish Institute of Space Physics, Kiruna, Sweden, Proceedings of the Sixth European Symposium on Stratospheric Ozone Research, Gothenberg, Sweden, 369–372, 2002.

Randall, C. E., Harvey, V. L., Siskind, D. E., France, J., Bernath, P. F., Boone, C. D., and Walker, K. A.: NO_x descent in the Arctic middle atmosphere in early 2009, Geophys. Res. Lett., 36, L18811, doi:10.1029/2009GL039706, 2009.

Randall, C. E., Harvey, V. L., Singleton, C., S., Bailey, S. M., Bernath, P. F., Codrescu, M., Nakajima, H., and Russell III, J. M.: Energetic particle precipitation effects on the southern hemisphere stratosphere in 1992–2005, J. Geophys. Res., 112, D08308, doi:10.1029/2006JD007696, 2007.

Randall, C. E., Harvey, V. L., Singleton, C. S., Bernath, P. F., Boone, C. D., and Kozyra, J. U.: Enhanced NO_x in 2006 linked to strong upper stratospheric Arctic vortex, Geophys. Res. Lett., 33, L18811, doi:10.1029/2006GL027160, 2006.

Randall, C. E., Harvey, V. L., Manney, G. L., Orsolini, Y., Codrescu, M., Sioris, C., Brohede, S., Haley, C. S., Gordley, L. L., Zawodny, J. M., and Russell, J. M.: Stratospheric effects of energetic particle precipitation in 2003–2004, Geophys. Res. Lett., 32, L05802, doi:10.1029/2004GL022003, 2005.

Rienecker, M. M, Suarez, M. J., Todling, R., Bacmeister, J., Takacs, L., Liu, H.-C., Gu, W., Sienkiewicz, M., Koster, R. D., Gelaro, R., Stajner, I., and Nielsen, J. E.: The GEOS-5 Data Assimilation System-Documentation of Versions 5.0.1, 5.1.0, and 5.2.0, Tech. Rep. 104606 V27, NASA, Greenbelt, MD, 2008.

Rienecker, M. M., Suarez, M. J., Gelaro, R., Todling, R., Bacmeister, J., Liu, E., Bosilovich, M. G., Schubert, S. D., Takacs, L., Kim, G.-K., Bloom, S., Chen, J., Collins, D., Conaty, A., da Silva, A., Gu, W., Joiner, J., Koster, R. D., Lucchesi, R., Molod, A., Owens, T., Pawson, S., Pegion, P., Redder, C. R., Reichle, R., Robertson, F. R., Ruddick, A. G., Sienkiewicz, M., and Woollen, J.: MERRA: NASA's Modern-Era Retrospective Analysis for Research and Applications, J. Climate, 24, 3624–3648, doi:10.1175/JCLI-D-11-00015.1, 2011.

Rodgers, C. D. and Connor, B. J.: Intercomparison of remote sounding instruments, J. Geophys. Res., 108, 4116, doi:10.1029/2002JD002299, 2003.

Ryan, N. J., Palm, M., Raffalski, U., Larsson, R., Manney, G., Millán, L., and Notholt, J.: Strato-mesospheric carbon monoxide profiles above Kiruna, Sweden (67.8 ° N, 20.4 ° E), since 2008, Earth Syst. Sci. Data, 9, 77-89, doi:10.5194/essd-9-77-2017, 2017.

Schoeberl, M. R., Lait, L. R., Newman, P. A., and Rosenfield, J. E.: The structure of the polar vortex, J. Geophys. Res., 97, 7859–7882, 1992.

Schwartz, M., Pumphrey, H., Livesey, N., and Read, W.: MLS/Aura Level 2 Carbon Monoxide (CO) Mixing Ratio V004, version 004, Greenbelt, MD, USA, Goddard Earth Sciences Data and Information Services Center (GES DISC), available at: doi:10.5067/AURA/MLS/DATA2005, last access: February 2017, 2015.

Siskind, D. E., Eckermann, S. D., McCormack, J. P., Coy, L., Hoppel, K. W., and Baker, N. L.: Case studies of the mesospheric response to minor, major and extended stratospheric warmings, J. Geophys. Res., 115, D00N03, doi:10.1029/2010JD014114, 2010.

Siskind, D. E., Nedoluha, G. E., Sassi, F., Rong, P., Bailey, S. M., Hervig, M. E., and Randall, C. E.: Persistence of upper stratospheric wintertime tracer variability into the Arctic spring and summer, Atmos. Chem. Phys., 16, 7957-7967, doi:10.5194/acp-16-7957-2016, 2016.

Smith, A. K., Garcia, R. R., Marsh, D. R., and Richter J. H.: WACCM simulations of the mean circulation and trace species transport in the winter mesosphere, J. Geophys. Res., 116, D20115, doi:10.1029/2011JD016083, 2011.

Solomon, S., Kiehl, J. T., Garcia, Grose, W.: Tracer Transport by the Diabatic Circulation Deduced from Satellite Observations, J. Atmos. Sci., 43, 15, 1603-1617, doi: http://dx.doi.org/10.1175/1520-0469(1986)043<1603:TTBTDC>2.0.CO;2, 1986.

Solomon, S., Garcia, R. R., Olivero, J. G., Bevilacqua, R. M., Schwarzt, P. R., Clancy, R. T., and Muhleman, D. O.: Photochemistry and Transport of Carbon Monoxide in the Middle Atmosphere, J. Atmos. Sci., 42(10), 1072-1083, 1985.

Straub, C., Tschanz, B., Hocke, K., Kämpfer, N., and Smith, A. K.: Transport of mesospheric H_2O during and after the stratospheric sudden warming of January 2010: observation and simulation, Atmos. Chem. Phys., 12, 5413–5427, doi:10.5194/acp-12-54132012, 2012.

Waters, J., Froidevaux, L., Harwood, R., Jarno, R., Pickett, H., Read, W., Siegel, P., Cofield, R., Filipiak, M., Flower, D., Holden, J., Lau, G., Livesey, N., Manney, G., Pumphrey, H., Santee, M., Wu, D., Cuddy, D., Lay, R., Loo, M., Perun, V., Schwartz, M., Stek, P., Thurstans, R., Boyles, M., Chandra, S., Chavez, M., Chen, G.-S., Chudasama, B., Dodge, R., Fuller, R., Girard, M., Jiang, J., Jiang, Y., Knosp, B., LaBelle, R., Lam, J., Lee, K., Miller, D., Oswald, J., Patel, N., Pukala, D., Quintero, O., Scaff, D., Snyder, W., Tope, M., Wagner, P., and Walch, M.: The Earth Observing System Microwave Limb Sounder (EOSMLS) on the Aura satellite, IEEE T. Geosci. Remote, 44, 1075–1092, 2006.

York, D., Evensen, N. M., Martinez, M. L., and Delgado, J. D. B.: Unified equations for the slope, intercept, and standard errors of the best straight line, Am. J. Phys., 72, 367–375, 2004.

Atmos. Chem. Phys. Discuss., https://doi.org/10.5194/acp-2017-557
Manuscript under review for journal Atmos. Chem. Phys.
Discussion started: 21 June 2017

Atmospheric Chemistry and Physics Discussions

reference	tracer	location	instrument platform	rate of vertical motion [m/day]	time of year	terminology
Allen at al. (2000)	CO	Antarctica	satellite	-250 to -330	Autumn, 1992	atmospheric descent
Forkman et al. (2005)	CO	NH mid-latitudes	ground-based	250 to 450	Spring, 2002	mesospheric circulation
Forkman et al. (2005)	CO	NH mid-latitudes	ground-based	up to -300	Autumn, 2002	mesospheric circulation
Nassar et al. (2005)	N2O, CH4, H2O	Arctic	satellite	-105 to -174	winter average, 2004	atmospheric descent
Nassar et al. (2005)	CH4, H2O	Arctic	satellite	-150	Feb/Mar, 2004	atmospheric descent
Funke et al. (2009)	CO	Arctic	satellite	-350 to 400	Sep/Oct, 2003	polar descent
Funke et al. (2009)	CO	Arctic	satellite	-200 to -300	Nov/Dec, 2003	polar descent
Funke et al. (2009)	CO	Arctic	satellite	-1200	after SSW, 2004	polar descent
Di Bagio et al. (2010)	CO	Arctic	ground-based	-200 to -300	after SSW, 2009	descent of air
Di Bagio et al. (2010), from Orsolini et al. (2010)	H2O	Arctic	ground-based	-200 to -300	after SSW, 2009	descent of air
Straub et al. (2012)	H2O	Arctic	ground-based	-350	Jan/Feb/Mar 2010	polar descent
Straub et al. (2012)	H2O	Arctic	satellite	-360	Jan/Feb/Mar 2010	polar descent
Bailey et al. (2014)	NO, H2O, CH4	Arctic	satellite	up to -1000	after SSW, 2013	atmospheric descent

Table 1: A partial list of studies that used atmospheric tracers to derive rates of vertical air motion in the atmosphere.

Atmos. Chem. Phys. Discuss., https://doi.org/10.5194/acp-2017-557
Manuscript under review for journal Atmos. Chem. Phys.
Discussion started: 21 June 2017

Atmospheric Chemistry and Physics Discussions

	KIMRA-MLS	KIMRA-MLSsmooth	KIMRA-WACCM	KIMRA-WACCMsmooth	MLS-WACCM	MLSsmooth-WACCMsmooth
86km	0.87, 0.95 ± 0.03	0.93, 1.26 ± 0.05	0.81, 1.05 ± 0.01	0.86, 1.25 ± 0.01	0.90, 1.00 ± 0.02	0.89, 0.93 ± 0.05
76km	0.90, 1.46 ± 0.03	0.94, 1.27 ± 0.03	0.89, 1.18 ± 0.01	0.89, 1.26 ± 0.01	0.91, 0.78 ± 0.01	0.87, 0.78 ± 0.02
66km	0.90, 1.27 ± 0.02	0.95, 1.36 ± 0.03	0.85, 1.20 ± 0.01	0.90, 1.26 ± 0.01	0.90, 0.83 ± 0.01	0.85, 0.72 ± 0.01
56km	0.91, 1.01 ± 0.02	0.95, 1.20 ± 0.02	0.88, 0.95 ± 0.01	0.90, 01.00 ± 0.01	0.89, 0.86 ± 0.01	0.86, 0.70 ± 0.01
46km	0.88, 0.38 ± 0.01	0.91, 1.23 ± 0.04	0.89, 0.30 ± 0.01	0.90, 0.95 ± 0.02	0.88, 0.86 ± 0.01	0.83, 0.63 ± 0.01

Table 2: "correlation coefficient, regression coefficient ± error" for comparisons of daily CO VMRs from KIMRA, MLS, and SD-WACCM above Kiruna for 2008 through 2014. The abscissa variable is the first-named of each instrument pairing. A regression coefficient > 1 (< 1) indicates a larger (smaller) range in the abscissa variable. Figure 1 shows the time-series' of each CO VMR dataset. See Sect. 2.4 for details.

Atmos. Chem. Phys. Discuss., https://doi.org/10.5194/acp-2017-557
Manuscript under review for journal Atmos. Chem. Phys.
Discussion started: 21 June 2017

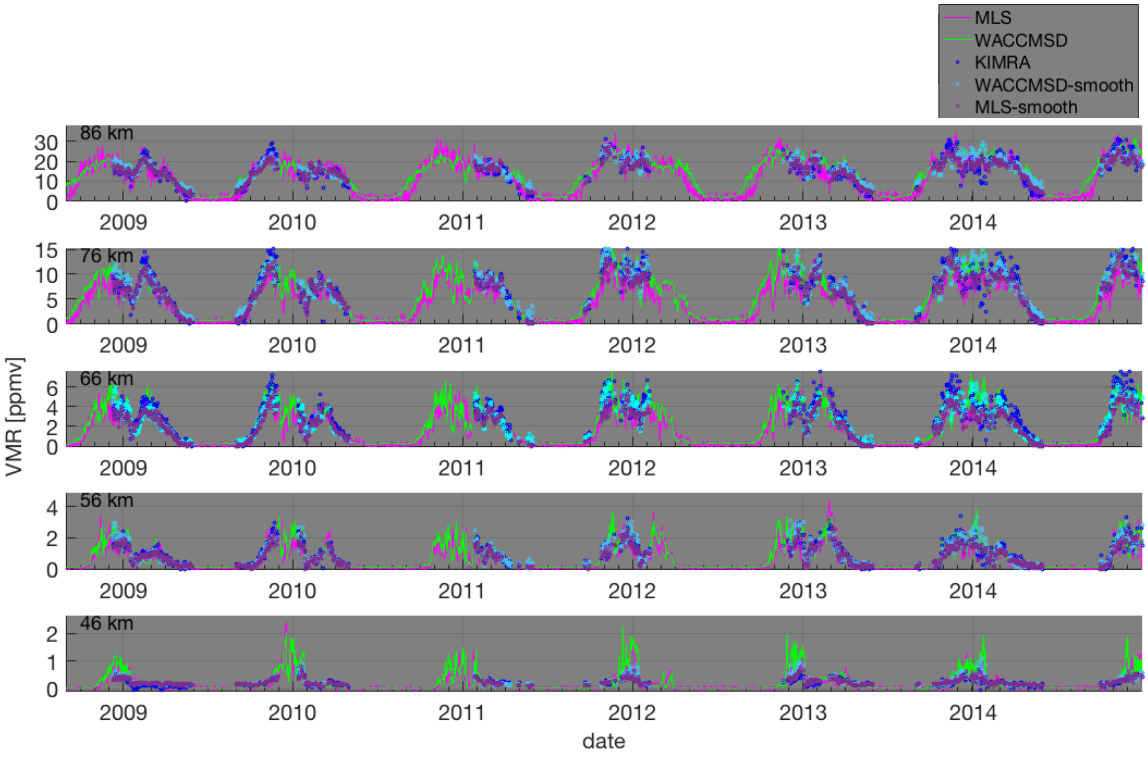

Figure 1: Comparisons of daily CO VMRs from KIMRA, MLS, and SD-WACCM above Kiruna for 2008 through 2014. Values are displayed at 46, 56, 66, 76, and 86 km. Correlation and regression coefficients for the datasets are given in Table 2. See Sect. 2.4 for details.

Atmos. Chem. Phys. Discuss., https://doi.org/10.5194/acp-2017-557
Manuscript under review for journal Atmos. Chem. Phys.
Discussion started: 21 June 2017

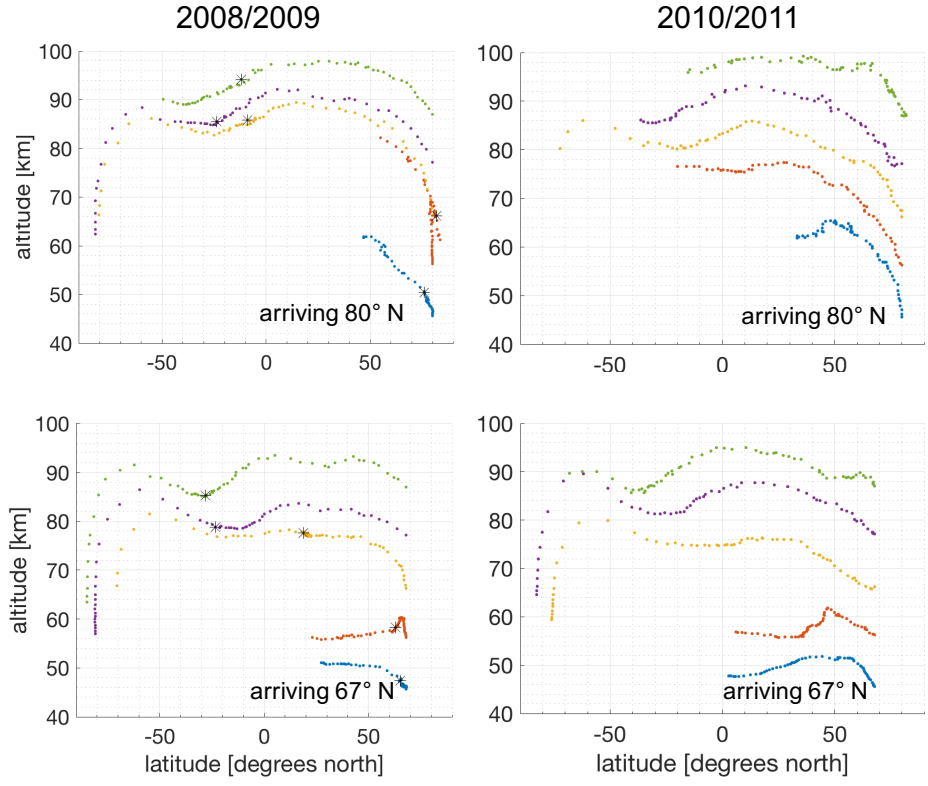

Figure 2: Trajectories of air parcels advected backwards 60 days in time from February 28th, 2009 and 2011, by the TEM circulation. Trajectories are calculated for air parcels arriving at 67° N and 80° N, at 46, 56, 66, 76, and 86 km altitude and locations are plotted at midnight each day. The start date of the 2009 SSW on 28th January is indicated with black stars. See Sect. 3 for more details.

Atmos. Chem. Phys. Discuss., https://doi.org/10.5194/acp-2017-557
Manuscript under review for journal Atmos. Chem. Phys.
Discussion started: 21 June 2017

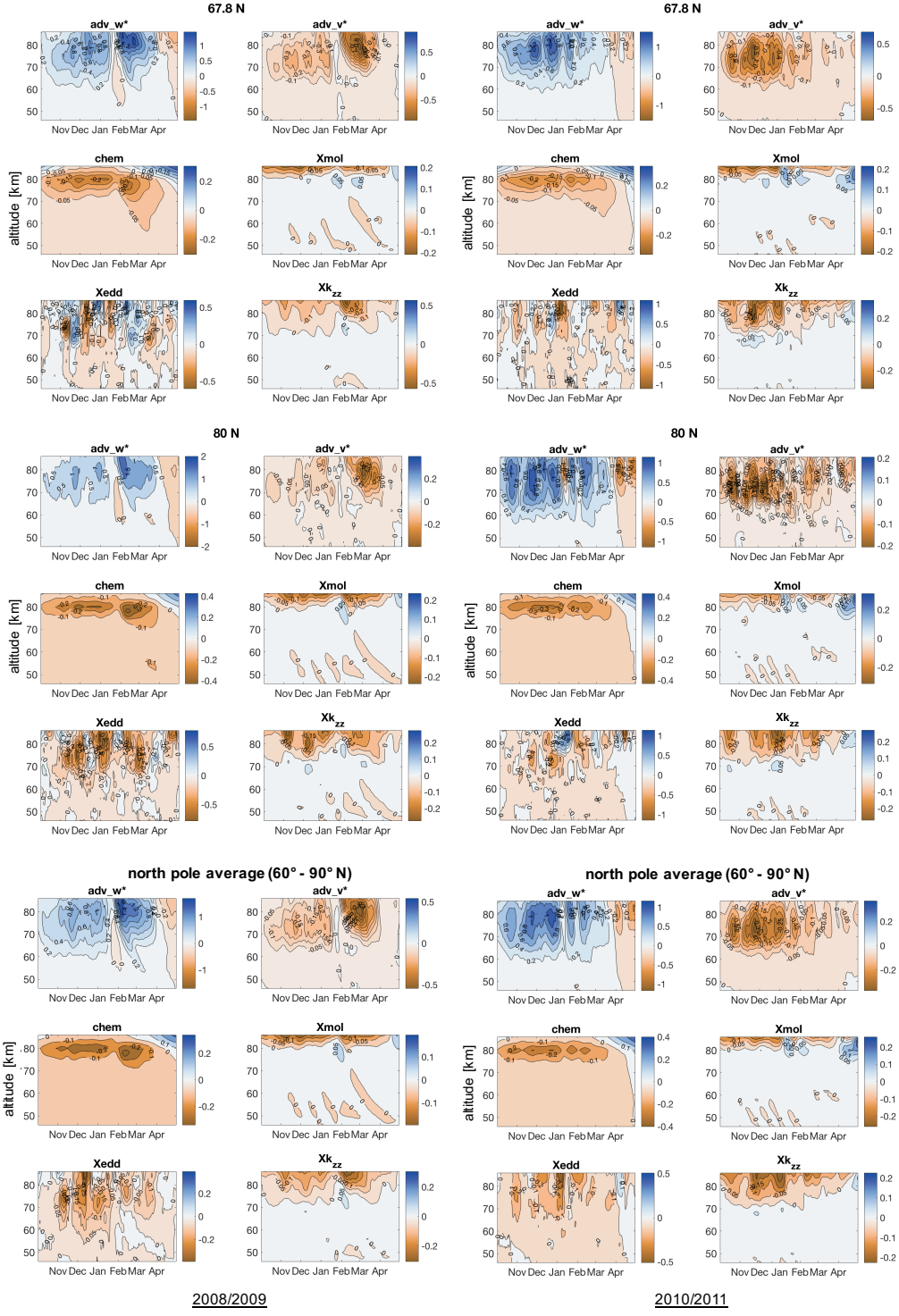

Figure 3: Tendencies of CO (in ppmv/day) for 67° N, 80° N, and north pole average (60° – 90° N) for the winters of 2008/2009 and 2010/2011. See section 2.4 for a description of the tendencies which are represented in the TEM continuity equation.

Atmos. Chem. Phys. Discuss., https://doi.org/10.5194/acp-2017-557
Manuscript under review for journal Atmos. Chem. Phys.
Discussion started: 21 June 2017

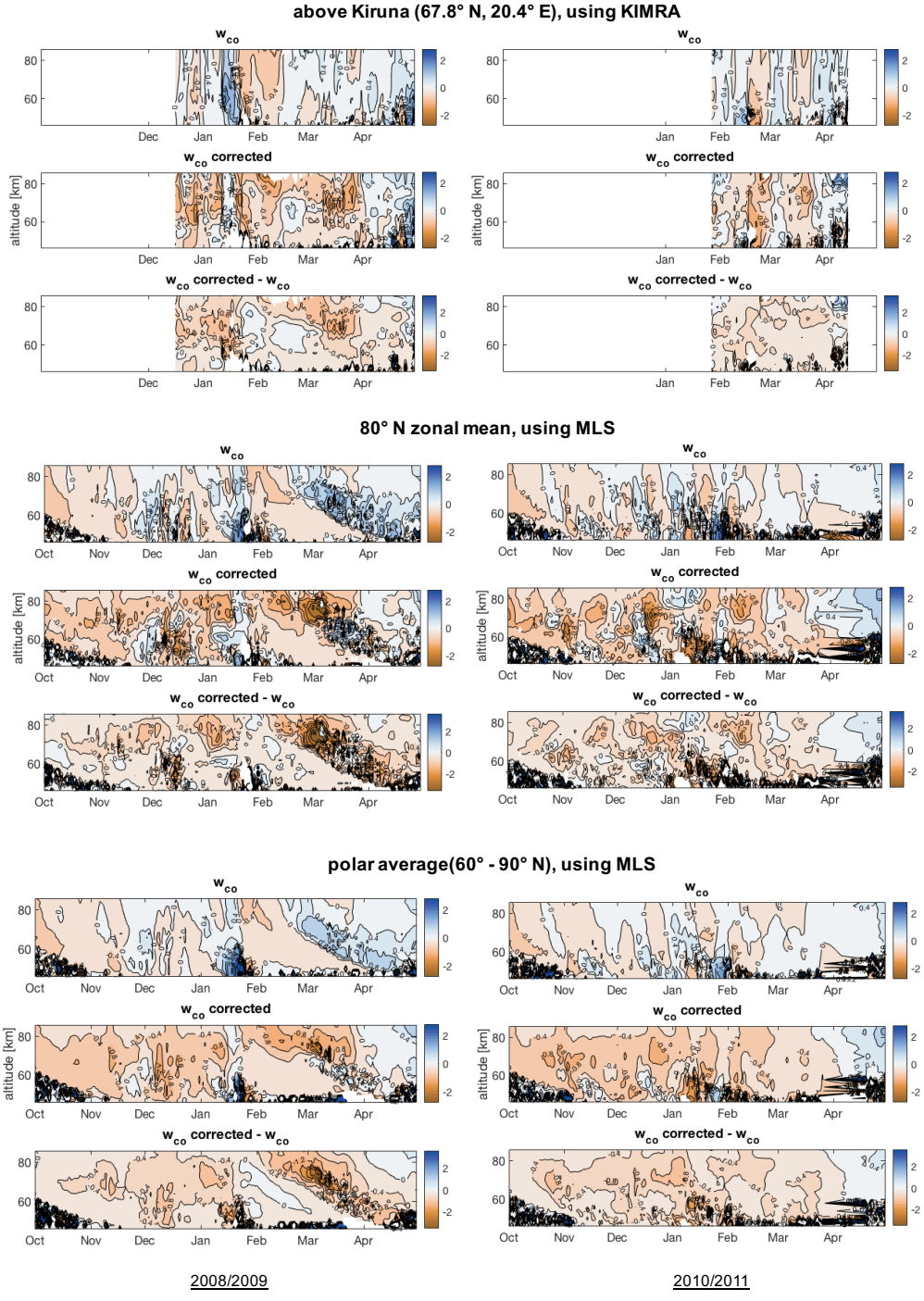

Figure 4: Rates of vertical motion, w_{CO}, in km/day, calculated using CO data from KIMRA and MLS (see Sect. 4). Contour lines are spaced by 0.2 km/day. KIMRA data is available from mid-December 2008, and late-January 2011. Areas with tightly packed contours (black areas) occur when there are very low CO VMRs and the calculation method is unreliable. White areas are where a CO VMR could not be tracked within the shown altitude range.

Atmos. Chem. Phys. Discuss., https://doi.org/10.5194/acp-2017-557
Manuscript under review for journal Atmos. Chem. Phys.
Discussion started: 21 June 2017

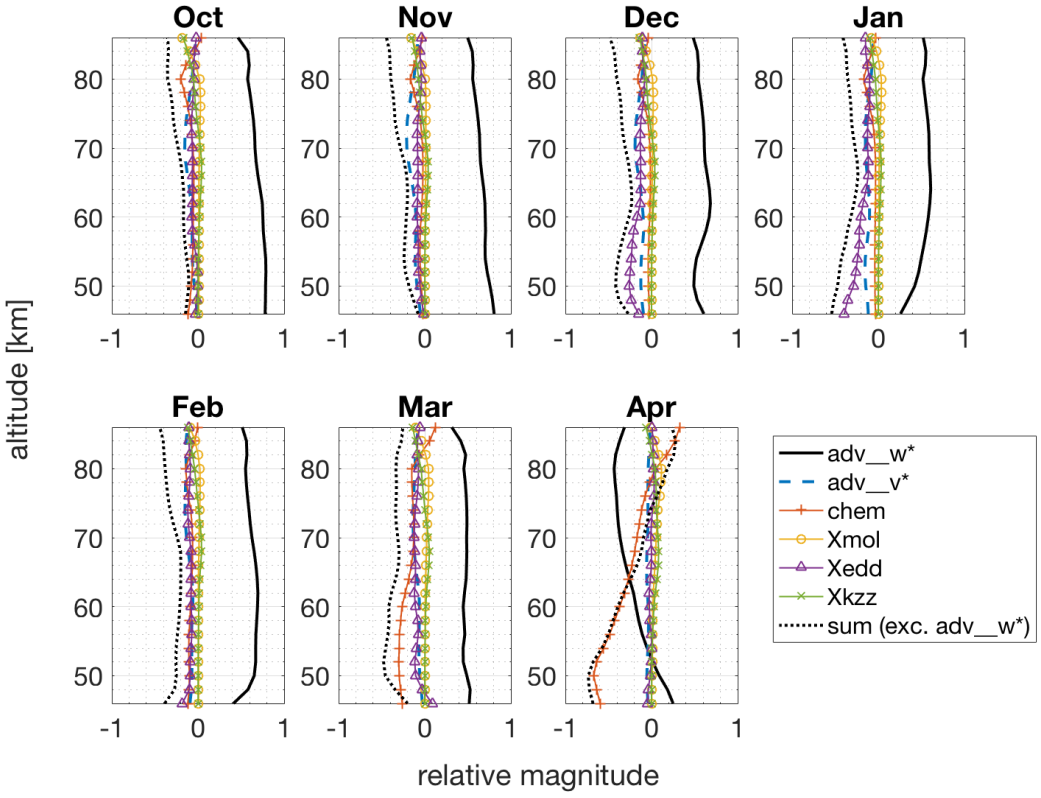

Figure 5: Monthly mean CO tendencies (Eq. (2)) over the north pole (60° – 90° N) around winter time, calculated using SD-WACCM data from January 2008 to April 2014. Model output corresponding to 10 days directly before and after a SSW, as well as the start-date, are excluded. The values are expressed relative to the to the monthly means of the absolute sum of all tendencies, and are referred to as relative strengths (Sect. 5). A strength of the sum of the tendencies, excluding adv_w*, is also plotted.

Atmos. Chem. Phys. Discuss., https://doi.org/10.5194/acp-2017-557
Manuscript under review for journal Atmos. Chem. Phys.
Discussion started: 21 June 2017

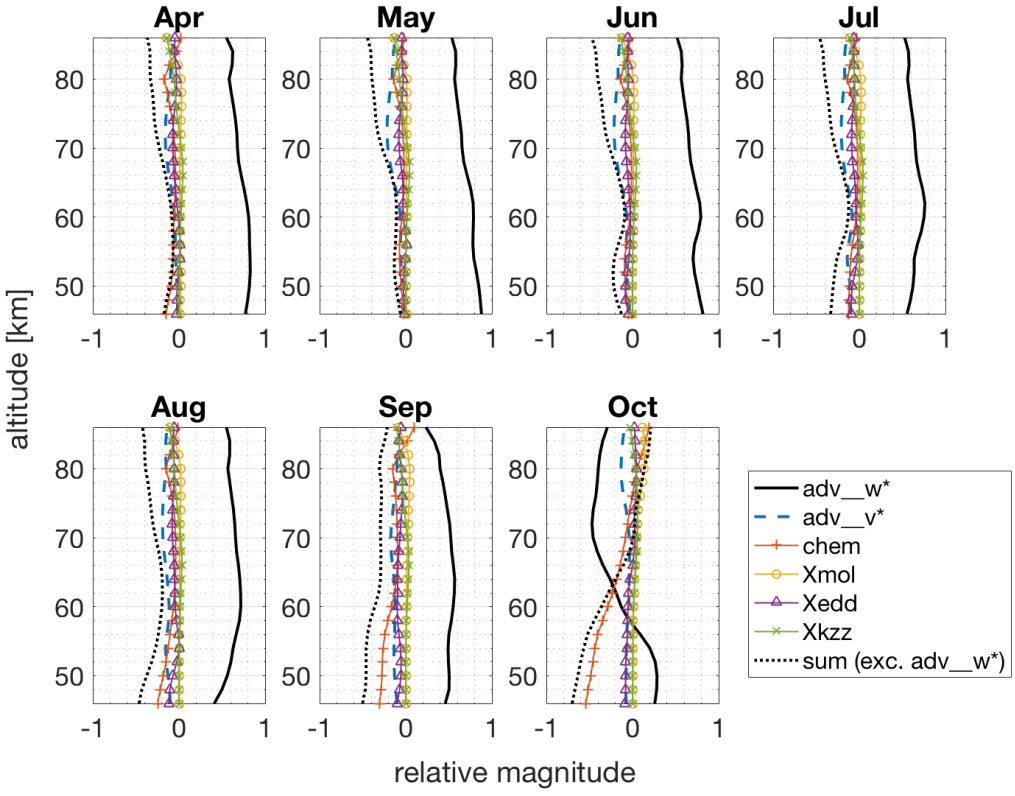

Figure 6: Same plots as for Fig. 5, but for the south pole (60° – 90° S), around the time of southern hemisphere winter, and with no exclusion of model output for SSWs.

Atmos. Chem. Phys. Discuss., https://doi.org/10.5194/acp-2017-557
Manuscript under review for journal Atmos. Chem. Phys.
Discussion started: 21 June 2017

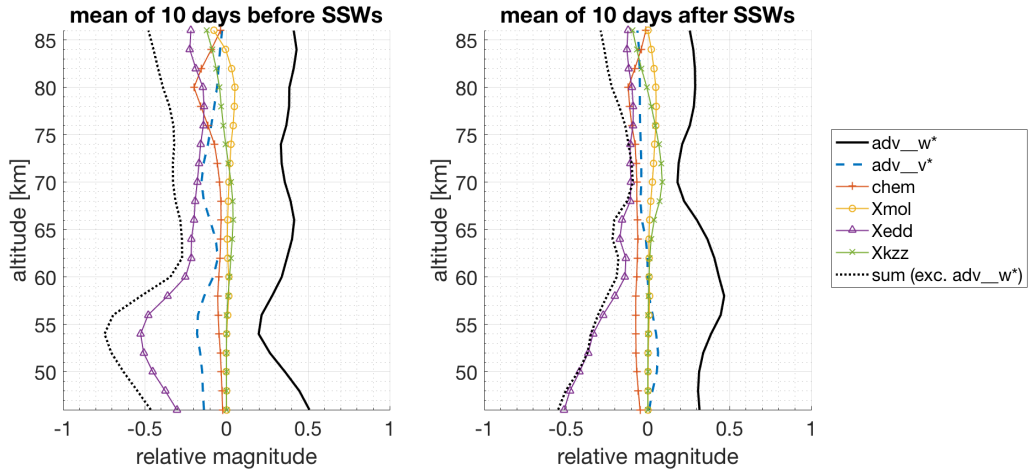

Figure 7: Same plots as for Fig. 5 (60 – 90 N), but for the 10 days directly before and after SSWs within Jan 2008 to April 2014. See Sect. 5 for details.

Atmos. Chem. Phys. Discuss., https://doi.org/10.5194/acp-2017-557
Manuscript under review for journal Atmos. Chem. Phys.
Discussion started: 21 June 2017

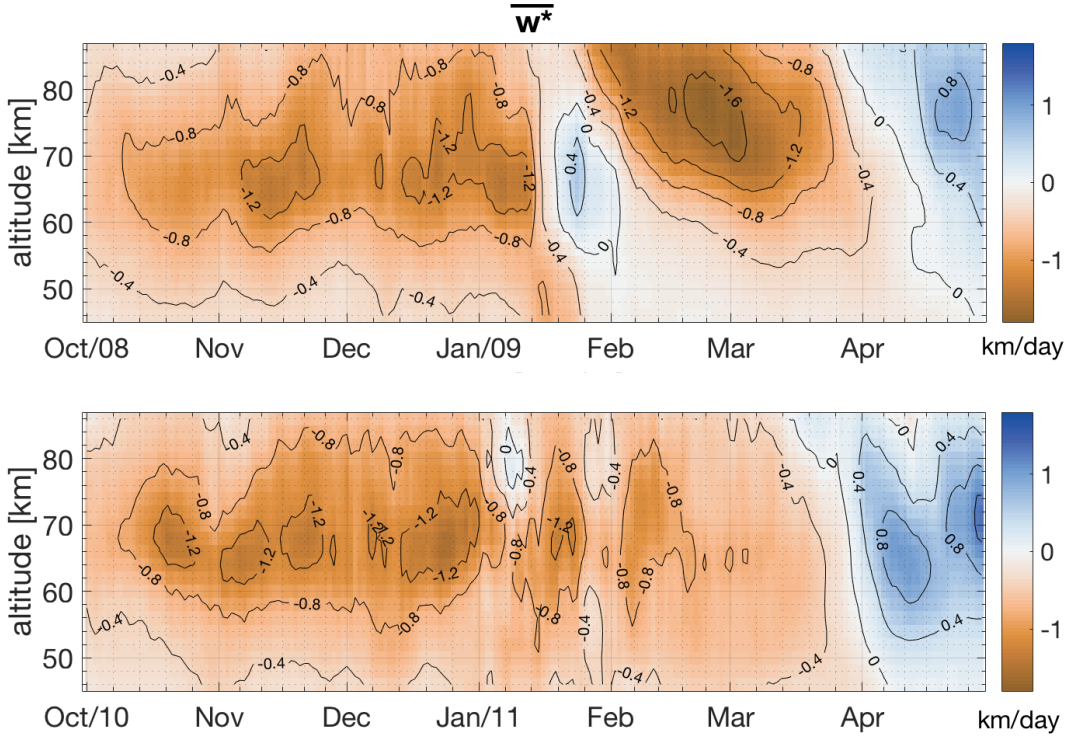

Figure 8: The north pole average (60° – 90° N) TEM vertical wind, $\overline{w}^*$, for the winters of 2008/2009, and 2010/2011. The values are calculated using daily output from SD-WACCM.